

AN EXPERIMENTAL CHECK ON PARTICLE DYNAMICS SIMULATIONS OF ERODIBLE PARTICLE BEDS; THE ROTATING TUMBLER.

Hung TRUONG^{1*}, John WELLS^{2*} and Anh NGUYEN¹

Dept. of Civil and Environmental Engineering, Ritsumeikan University
(Noji Higashi 1-1-1, Kusatsu, Shiga 525-8577, Japan)
E-mail:jwells@se.ritsumei.ac.jp

¹ Graduate student, ² Associate Professor, * Member of JSCE

To numerically simulate “bedload transport” of sediment by a turbulent flow over an erodible bed, our group has been developing “fictitious domain” methods to handle dense-phase particulate flow in turbulent flow of liquid. We report on efforts to check our simulation method against experiment for a dense-phase particulate flow in liquid, namely a rotating drum half-filled with spherical particles. Overall agreement between experimental and simulated values of static and dynamic angle of repose is found to be quite satisfactory, both in air and in oil.

Key Words : *bedload transport, numerical simulation, turbulence, DEM, rotating drum*

1. INTRODUCTION

Our group aims to numerically simulate “bedload transport” of sediment by a turbulent flow over an erodible bed. Passing up through the bedload layer, the mechanism resisting flow transitions rapidly from interparticle contacts/collisions to turbulent momentum transport. This juxtaposition necessitates both 1) tracking $O(1000)$ 3D particles in the manner of Particle Dynamics Simulations, with appropriate modeling of contact and “lubrication” forces, and 2) (given the absence of reliable turbulence models for dense two-phase flow) resolving all stress-supporting scales of the turbulence, which in the bedload layer means resolving eddies having a characteristic size comparable to the particle diameter, possibly less. *If* the reliability of such “quasi-direct” simulations can be proved, we can *then* proceed to investigate how bed shear drives sediment flux, how sand becomes suspended, how bed particles are sorted by size or density, how bed ripples form, and so on.

Given their obvious potential benefits, several groups have performed particle dynamics simulations of bedload transport, first in air¹⁾ and then in water^{2),3),4)}, and thus some of the above-mentioned phenomena have been partially considered. We are attempting significantly greater detail and fidelity in our simulations, which accordingly will include the following capability:

- Resolution of turbulent flow in space and time, so that inhomogeneities in the stream and span directions may be handled.
- Nearly fully-resolved instantaneous flow around particles, so that point models of fluid force, the accuracy of which is very doubtful, are not required.
- Experimentally verified models for lubrication forces and interparticle contact forces.

By rigorously checking each component of our simulation, and assigning bounds to the errors involved, we hope to approach closely to the ideal of “direct” numerical simulations, the results of which can be trusted to a high degree. The present paper reports on efforts to check our simulation method against experiment for a dense-phase particulate flow in liquid, with corresponding tests also performed in air. As an experimentally convenient test case which captures important aspects of bedload transport, we chose a rotating drum half-filled with spherical particles. This configuration has become popular in studies of granular flow dynamics⁵⁾, and as a benchmark for DEM simulations in air⁶⁾. Part of the present paper parallels such benchmarking. Concerning the liquid-immersed case, Jain et al. have recently contrasted phenomena observed experimentally in air and glycerine in a rotating tumbler⁷⁾. The present simulation results complement

some of their findings, as described below. We believe that the present paper is the first to use the liquid-immersed rotating tumbler as a benchmark for particle dynamics simulations.

2. FICTITIOUS DOMAIN METHOD

We are interested in the scientifically important transition from hydraulically smooth to rough sediment beds, which corresponds to particle Reynolds numbers, based on relative velocity, from 10 to a few hundred. In the upper half of this range, the requirements set out in the last section impose a lower limit on resolution of $O(10)$ grid points per diameter. Realistic computing resources do not yet suffice to apply boundary-fitted techniques to thousands of moving particles in 3D, so we must exploit fixed-grid “fictitious-domain” techniques; a standard incompressible Navier-Stokes solver is applied on a uniform Cartesian grid, but is modified to recover rigid body motion inside the moving and rotating particles by adding body forces to the governing equation.

Within the fictitious domain framework, Kajishima⁸⁾ has proposed to simply force the velocity field, to match rigid motion within particles, in proportion to the solid volume fraction in a given momentum cell. This efficient algorithm has permitted calculating the motion of 1000 or more solid particles in a turbulent flow, with particle Reynolds number in the range 10~300. Even at the rough resolution of 8 to 10 grid points per particle, Kajishima reports values of drag past a fixed sphere that approximate experimentally observed values well over a wide range of Re . Subsequent work^{9),10)} has shown that forcing at Lagrangian markers at the particle surface and within the particle achieves greater accuracy, but at a significant cost in computational time. Accordingly, Truong et al. have combined marker and volumetric forcing; the former is applied at particle surfaces, the latter within particles. In this way, the no-slip condition at particle surfaces is better satisfied than with pure volumetric forcing, but at modest computational cost. Since the effects of particle acceleration should be important during interparticle collisions and vortex entrainment, we apply a variable-density incompressible flow solver; tests reported in that work¹⁰⁾ showed that this approach does indeed predict particle acceleration better than when using a constant-density solver as done by previous workers.

(1) Particle- Fluid interaction

We apply a hybrid method of volumetric and marker velocity-based forcing, called “VIV-VIM”¹¹⁾

for solving the interaction between particle and fluid phase. In this method, the particle phase is treated as a fluid whose density equals that of the solid, but an artificial body force \bar{f}_p redistributes momentum within each particle at the end of a time step so as to recover rigid motion. Thus the particle-fluid system is treated as a variable-property fluid governed by the incompressible Navier-Stokes equations:

$$\frac{D(\rho\bar{u})}{Dt} = \nabla \cdot (\bar{p} + \mu[\nabla\bar{u} + (\nabla\bar{u})^T]) + \rho\bar{g} + \bar{f}_p \quad (1)$$

$$\nabla \cdot \bar{u} = 0 \quad (2)$$

where ρ and μ are respectively density and viscosity, which are taken to vary between liquid and solid according to a somewhat smoothed distribution. In the VIV-VIM method, the artificial body force \bar{f}_p is specified as:

$$\bar{f}_p(\bar{x}) = \alpha\rho\frac{(\bar{u}_p(\bar{x}) - \bar{u}(\bar{x}))}{\Delta t} + \sum \delta(\bar{X}_m - \bar{x})\bar{F}(\bar{X}_m) \quad (3)$$

In this equation, α is the solid volume fraction and \bar{u} is the partial-step velocity in a grid cell. $\bar{F}(\bar{X}_m)$ is the force specified at marker locations \bar{X}_m by :

$$\bar{F}(\bar{X}_m) = \rho_p h^3 \frac{(\bar{U}_p(\bar{X}_m) - \bar{U}(\bar{X}_m))}{\Delta t} \quad (4)$$

where $\bar{U}(\bar{X}_m) = \sum \bar{u} \delta(\bar{X}_m - \bar{x}) h^3$ is the fractional-step marker velocity which is interpolated from nearby grid cells by Peskin’s¹²⁾ discretized Dirac delta function δ , h is the grid spacing, $\bar{u}_p = \bar{U}_p + \bar{\Omega}_p \times \bar{r}$ is the particle’s target velocity at a grid point, \bar{r} is the vector pointing from the particle center \bar{X}_p to the cell center; $\bar{U}_p(\bar{X}_m)$ is the marker target velocity defined by :

$$\bar{U}_p(\bar{X}_m) = \bar{U}_p + \bar{\Omega}_p \times (\bar{X}_m - \bar{X}_p) \quad (5)$$

where \bar{U}_p and $\bar{\Omega}_p$ are particle’s translational and angular velocities.

(2) Particle- Particle interactions

To treat inter-particle contacts, and equivalently particle-wall contacts, we employed a DEM method¹³⁾ which is now briefly described. The normal and tangential components of contact force between particles i and j , denoted by the subscripts n and t respectively, are modeled as:

$$\bar{f}_{nij} = -\kappa_n \bar{\delta}_{nij} - (\eta_n \bar{v}_{rij} \cdot \bar{n}_{ij}) \bar{n}_{ij} \quad (6)$$

$$\bar{f}_{tij} = -(\kappa_t \bar{\delta}_{tij} + \eta_t \bar{v}_{sij}) \quad (7)$$

where κ and η are stiffness and damping coefficients, $\bar{\delta}$ is the displacement vector, \bar{v}_{rij} is the velocity of the particle i relative to particle j , \bar{v}_{sij} is the slip velocity of the contact point and \bar{n}_{ij} is the unit vector pointing from the center of particle i to that of particle j . When the tangential force \bar{f}_{ij} satisfies $|\bar{f}_{ij}| > k|\bar{f}_{nij}|$, \bar{f}_{ij} is replaced by:

$$\bar{f}_{ij} = -k|\bar{f}_{nij}|\bar{v}_{ij}/|\bar{v}_{ij}| \quad (8)$$

where k is the coefficient of friction, taken to be 0.5 in the present simulations.

3. NUMERICAL SIMULATION

(1) Computational setup

The rotating drum apparatus, which contains solid particles and possibly an interstitial liquid, is modeled as a cylindrical region embedded in a 3D Cartesian computational grid as shown in fig. 1. In the dry case, denoted below by ‘‘air’’, the cylinder was represented in terms of its bounding surfaces, which took the role of particle j in equations (6-8) when contacting other particles i .

For the liquid-immersed case, the drum boundary is additionally represented, for the purpose of the flow calculation, as a set of discretized markers that are distributed over the drum surface. The distance between two connected markers is set to half or one grid spacing. The outer region of the drum is assumed to be filled with the same fluid as that of the inner region. Thus governing equations for the fluid phase can be solved in a fixed grid over the entire domain while the target velocity at the drum boundary is imposed by evaluating the Lagrangian force at every boundary marker and spreading to the Eulerian grid.

With the exception of step **P1** below, the following describes the algorithm for the liquid-immersed computations.

The target velocity at boundary maker i is given by :

$$\bar{U}_b(\bar{X}_m^b) = \bar{R}_m \times \bar{W} \quad (9)$$

where $\bar{R}_m = (X_m^b - X_G, Y_m^b - Y_G, 0)$ and $\bar{W} = (0, 0, \Omega_b)$; $\bar{X}_G = (X_1/2, Y_1/2, Z_1/2)$ is the center and Ω_b is the angular velocity of the drum.

The Lagrangian force at a marker is specified as:

$$\bar{F}_b(\bar{X}_m) = \rho_f h^3 \frac{(\bar{U}_b(\bar{X}_m^b) - \bar{U}(\bar{X}_m))}{\Delta t} \quad (10)$$

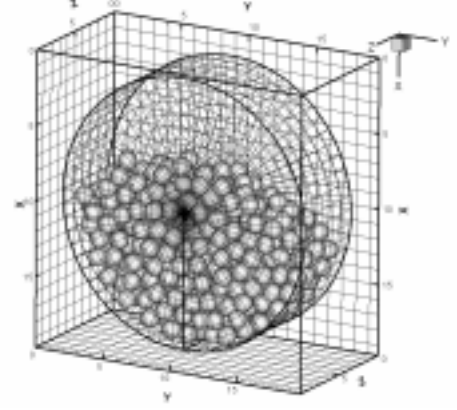


Fig. 1 Fixed grid for the Cartesian domain and Langrangian grid for the cylindrical rotating drum; boundary markers are distributed at the Langrangian grid nodes.

and is transferred to the fixed Eulerian grid by :

$$\bar{f}_b = \sum \delta(\bar{X}_m^b - \bar{x}) \bar{F}_b(\bar{X}_m^b) \quad (11)$$

(2) Numerical scheme

A finite-difference method based on a staggered grid and central differences in space is employed to solve the variable density Navier-Stokes equations¹⁴. Equation (1) is discretized from time level n to time level $n+1$ by forward Euler method as:

$$\frac{\rho^{n+1}\bar{u}^{n+1} - \rho^n\bar{u}^n}{\Delta t} + \bar{A}^n = \bar{F}^n - \nabla\phi^{n+1} + \bar{f}^{n+1} \quad (12)$$

where Δt is the time step, ϕ^{n+1} is the pseudo-pressure, $\bar{A}^n = \nabla_h \cdot \rho^n \bar{u}^n \bar{u}^n$ is the momentum advection term and

$\bar{F}^n = \nabla_h \cdot \mu^n (\nabla_h \bar{u}^n + \nabla_h^T \bar{u}^n) - \nabla_h p^n + \rho^n \bar{g}$ is the intensive fluid force.

Substeps for the fluid (‘‘F’’) phase, particle (‘‘P’’) phase and boundary (‘‘B’’) are as follows:

P1) Update particle positions to t^{n+1} , detect particle contacts and update particle velocity.

Because particles may contact at the time scale smaller than that of the fluid flow, we use shorter time interval for this step. Thus, to step a particle from time t^n to t^{n+1} , we need to perform N substeps which consist of the following tasks:

a) Advance particles from sub-step k to $k+1$ as :

$$\bar{X}_p^{n+1,k+1} = \bar{X}_p^{n+1,k} + \Delta t \bar{U}_p^{n+1,k} \quad (13)$$

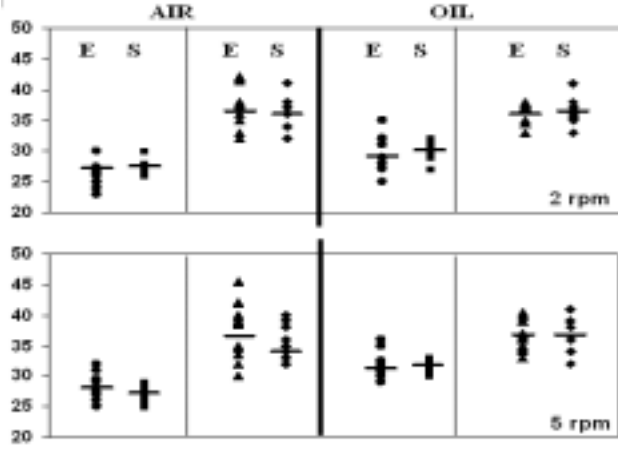


Fig. 2 Comparisons between (E)xperiment and (S)imulation of the dynamic and static angles of repose for 2 and 5 r.p.m. rotation speeds in air and oil.

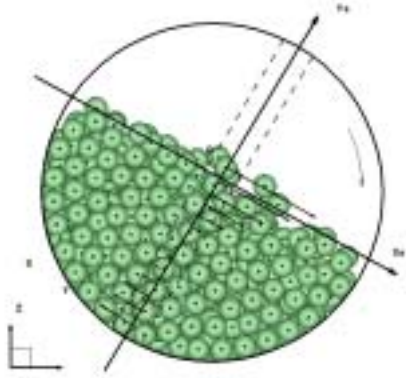


Fig. 3 Definition sketch of the bed-aligned coordinate system attached to the drum center. Black arrows indicate locally averaged particle velocity .

b) Search for particle contacts, thereafter calculate the contact force $\bar{F}_c^{n+1,k+1}$ and torque $\bar{T}_c^{n+1,k+1}$. When the number of particles is large, this step is time consuming, therefore a suitable particle contact searching algorithm must be employed. In the present scheme, a cell linked list method¹⁵⁾ is used .

c) Calculate particle translational and angular velocities at substep $k+1$ as:

$$\bar{U}_p^{n+1,k+1} = \bar{U}_p^{n+1,k} + \frac{\Delta t}{N} \frac{\bar{F}_c^{n+1,k+1}}{M_p} \quad (14)$$

$$\bar{\Omega}_p^{n+1,k+1} = \bar{\Omega}_p^{n+1,k} + \frac{\Delta t}{N} \frac{\bar{T}_c^{n+1,k+1}}{I_p} \quad (15)$$

P2) Based on the updated particle velocity, calculate the added force and update the fluid velocity field, and then calculate the new density and viscosity

fields ρ^{n+1} and μ^{n+1} .

F1) Calculate the momentum advection term \bar{A}^n and the intensive fluid force \bar{F}^n in each momentum cell.

F2) Obtain the “fractional-step” momentum density $\rho^{n+1}\bar{u}$ by subtracting the momentum advection term \bar{A}^n :

$$\rho^{n+1}\bar{u} = \rho^n\bar{u} + \Delta t (\bar{F}^n - \bar{A}^n) \quad (16)$$

and thence the fractional step velocity \bar{u} .

F3) Project \bar{u} to obtain a solenoidal velocity field :

$$\bar{\tilde{u}} = \bar{u} - \frac{\Delta t}{\rho^{n+1}} \nabla \phi \quad (17)$$

where ϕ satisfies the following elliptic equation :

$$\nabla_h \cdot \left(\frac{1}{\rho^{n+1}} \nabla_h \phi \right) = \frac{\nabla_h \cdot \bar{u}}{\Delta t} \quad (18)$$

The pressure field is then updated by:

$$p^{n+1} = p^n + \phi^{n+1} \quad (19)$$

P3) Within each particle, calculate the body force \bar{f}_b by equation (3) and add to the fluid to yield a rigidified momentum density $\rho^{n+1}\bar{u}^{n+1}$

$$\rho^{n+1}\bar{u}^{n+1} = \rho^{n+1}\bar{u} + \Delta t \bar{f}_p^{n+1} \quad (20)$$

B) Impose the target velocity at the drum boundary by calculating the body force \bar{f}_b by equation (11) and adding it to the fluid.

4. EXPERIMENT

(1) Experimental procedure

We recorded movies of the motion of 338 roughened glass spheres ($\phi 12.5$) occupying about half of a closed circular drum that was rotated around a horizontal axis at rates (Ω_b) ranging from 2 to 6 rpm, the maximal value obtainable with the apparatus. Experiments were performed with air and sunflower oil as the interstitial fluids. The internal dimensions of the vessel are 179.4 mm in diameter and 45.6 mm in width; bead diameter was $d = 12.5$ mm, about one quarter the vessel depth. The front and rear walls are glass, allowing optical access from the front, and a black background surface lies behind the rear glass plate. The outer wall is made of acrylic resin and has a 14 mm-diameter port through which particles and liquid are introduced. Temperature of

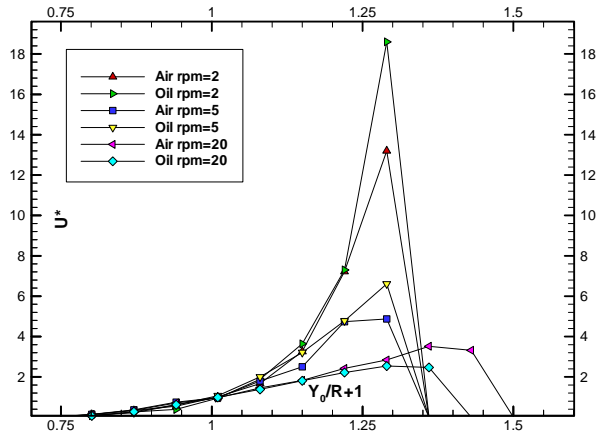


Fig. 4 Velocity profiles in the flowing layer. The horizontal axis is the layer height and the vertical one is the mean velocity nondimensionalized by ΩR . (Zero velocities to the right of the bed surface are artifacts.)

the air and oil during experiments was 25.5 ± 0.5 °C. Density of sunflower oil at 25 °C is 0.919 g/cm^3 and its kinetic viscosity is $70. \text{ mm}^2/\text{s}$. There was a 1.0 degree increase in temperature during runs with sunflower oil. Density of the beads is 2.49 g/cm^3 .

A Kodak ES 1.0 camera, with 1008x956 pixel resolution, was used to image the whole drum at 30 frames/sec for runs of 702 images. Recording started after the beads began to avalanche quasi-periodically.

(2) Image analysis

At the rather low rotation rates available with the apparatus, beads avalanched intermittently, and usually settling into a static state of rigid rotation before the next avalanche occurred. No sliding of beads against the wall was observed with the frosted beads, unlike smooth glass beads that were used in early trials and which resulted in frequent bulk backsliding instead of avalanching.

Instantaneous slope of the bead surface was determined visually, and was taken equal to that of a line that seemed to best approximate the bead surface in the central 80 % of the drum. This bed slope was determined when the bed slope peaked immediately before avalanching, and when the minimum value was observed as the avalanche was losing strength. The former will be termed the “static angle of repose”, while the latter value is believed to provide a close lower bound for the “dynamic angle of repose”^(6,7). The results were collected from runs at rotation speeds of 2 and 5 r.p.m. for both air and sunflower oil.

5. RESULTS AND DISCUSSION

The conditions of simulation matched those of the experimental runs at 2 and 5 r.p.m. After the drum completed one turn, 300 snapshots of particle positions and velocities were recorded. These snapshots were then used to calculate several averaged quantities. Animations were produced, and these were analyzed visually, in the same way as the experimental movies and by the same person, to determine static and dynamic angles of repose. The time-averaged velocity profile and flowing layer thickness were determined automatically as described below.

(1) Angle of repose

The static and dynamic angles of repose are reported in Fig. 2 for oil at 2 and 5 r.p.m. Overall agreement is seen to be quite satisfactory, both in air and in oil. In some cases, the sample variances appear to be rather different between experiment and simulation. This may be a result of the limited sample sizes.

(2) Velocity profile and flowing layer thickness

Using an approximate bed angle calculated automatically by the analysis program, the time-averaged streamwise velocity profile along a strip of width W , and height of $2R$ perpendicular to the bed surface at the center of the drum (see Fig. 3) is obtained as follows. The strip is divided into N_s sub-layers corresponding to N_s data points of the velocity profile. The velocity of a sub-layer is averaged over all particles whose centers lie on its regions from 300 snapshots.

For determining the flowing layer thickness, we slide a box along the strip while calculating its averaged velocity. We define the flowing layer thickness to be the distance from the flowing layer surface to the box whose absolute averaged velocity is minimum.

The calculated velocity profiles for different cases are plotted in Fig. 4. At rotation speeds of 2 rpm and 5 rpm, the maximum velocities at the flowing layer surface in oil are much higher than those in air. This could be explained by induced flow of the oil. As they start avalanching, the particles near the surface forming a large vortex (see Fig. 5) which later helps the particles to maintain their velocity. However, at the rotational speed of 20 r.p.m., we have observed the opposite phenomenon. The maximum velocity at the flowing surface in oil is smaller than that in air, possibly due to the increase of the fluid drag force acting on the particles. At higher rotation rate,

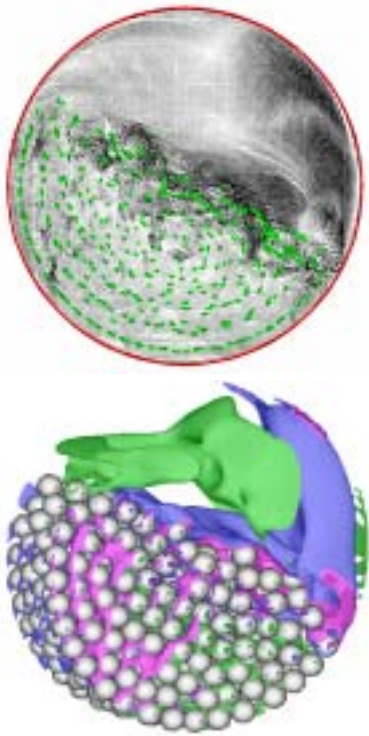


Fig. 5 Velocity vector field in a plane section at the center of the filled-oil rotating drum (top) and isosurfaces of velocity magnitudes in the range [1;12] (bottom) at $\Omega = 5r.p.m.$

Table 1. Thickness and maximum velocity at the surface of the flowing layer.

r.p.m.	δ / d		$U_{\text{surface}} / \Omega R$	
	Air	Oil	Air	Oil
2	3.76	3.65	13.64	18.6
5	3.77	3.67	4.87	6.61
20	4.68	4.17	3.52	2.54

the increased flowing layer thickness (see Table 1) leads to a lower particle concentration in this layer and therefore gives rise to the role of pore fluid.

6. CONCLUSIONS

The present paper is, to our knowledge, the first to use the liquid-immersed rotating tumbler as a benchmark for particle dynamics simulations. The overall agreement between experimental and simulated values for static and dynamic angles of repose and is found to be quite satisfactory, both in air and in oil. These preliminary results make us hopeful that our fictitious-domain simulation method is indeed suitable for simulating dense-phase granular flow in a liquid. The detail afforded by such simulations also opens up many possibilities for the scientific analysis of flow in this configuration. In the future, benchmark tests that involve coupling

between a turbulent shear flow and granular flow are desirable and necessary.

ACKNOWLEDGMENT

This work has been supported by the Environmental Flows Research Group at Ritsumeikan University. We thank graduate student Thien Duy NGUYEN for his expert help with experiments, and to Mr. T. YAMAUE for designing and maintaining the rotating drum apparatus.

REFERENCES

- 1) Werner, B.T., Haff, P.K., The impact process in aeolian saltation: Two-dimensional simulations, *Sedimentology*, 35, 189-196, 1988.
- 2) Schmeeckle, M. W., The Mechanics of Bedload Sediment Transport: Ph.D. dissertation, Univ. of Colorado, 158 p, 1998.
- 3)Gotoh, H., Harada, E., Sakai, T.: Movable bed simulator for fractional transport of graded sediment, *水工学論文集*, Vol. 44, 665-670,2000
- 4) Drake, T.G., Calantoni J. : Discrete particle model for sheet flow on the near shore, *Journal of Geophysical Research - Oceans*, 106-C9, 19859-19868,2001.
- 5) Nakagawa M., Altobelli, S.A., Caprihan, A., Fukushima E., Jeong, E. K., Noninvasive measurements of granular flows by magnetic resonance imaging, *Exp. Fluids*, 12,54, 1993.
- 6) Yamane, K., Nakagawa, M., Altobelli, S.A., Tanaka, T., Tsuji, T.: Steady particulate flows in a horizontal rotating cylinder, *Physics of Fluids*, Vol. 10, 6, 1998.
- 7) Jain, N., Ottino, J.M., Lueptow R.M., Effect of interstitial fluid on a granular flowing layer, *J. F. Mech.*,508, 23-44, 2004.
- 8) Kajishima, T., Takiguchi, S. : Interaction between particle clusters and particle-induced turbulence, *Int.J. Heat Fluid Flow* 23, 639-646, 2002
- 9) Uhlmann, M.: An immersed boundary method with direct forcing for the simulation of particulate flows, *J. Comput. Phys.* , 209,448-476, 2005.
- 10) Truong, H.V., Wells, J.C. , Tryggvason, G. : Explicit vs. implicit particle-liquid coupling in fixed-grid computations at moderate particle Reynolds number, FEDSM2005-77206, *ASME FED Summer Meeting*, June 19-23,2005, USA
- 11) Truong, H.V., Wells, J.C. , Tryggvason, G. : Implicitly - coupled finite difference schemes for fictitious domain simulation of solid-liquid flow; marker, volumetric, and hybrid forcing, *ERCOFTAC workshop*, DLES6 Sept.,2005, France.
- 12) Peskin, C.S., The immersed boundary method, *Acta numerica*, 11, 479-517, 2002.
- 13) Tsuji, Y., Tanaka, T., Ishida, T. Lagrangian numerical simulation of plug flow of cohesionless particles in horizontal pipe, *Powder technology* 71, pp 239-250, 1992.
- 14) Tryggvason, G., Brunner, B., Esmaeili, A., Juric, D., Alrawashi, N., Tauber, W., Han, J., Nas, S., Jan, Y.J. : A front tracking method for the computations of multiphase flow, *J. Comput. Phys.*, 169, 708-759, 2001.
- 15) Allen, M.P., Tildesley, D. : Computer simulation of liquids, Clarendon Press, Oxford 1987.

(Received September 30,2005)